Anatomy of the symmetry energy of dilute nuclear matter

J. N. De,* S. K. Samaddar,† and B. K. Agrawal‡
Saha Institute of Nuclear Physics, 1/AF Bidhannagar, Kolkata 700064, India
(Received 2 August 2010; published 8 October 2010)

The symmetry energy coefficients of dilute clusterized nuclear matter are evaluated in the S-matrix framework. Employing a few different definitions commonly used in the literature for uniform nuclear matter, it is seen that the different definitions lead to perceptibly different results for the symmetry coefficients for dilute nuclear matter. They are found to be higher compared to those obtained for uniform matter in the low density domain. The calculated results are in reasonable consonance with those extracted recently from experimental data.

DOI: 10.1103/PhysRevC.82.045201 PACS number(s): 21.65.Cd, 21.30.Fe, 21.65.Ef, 24.10.Pa

I. INTRODUCTION

Experiments [1,2] have recently been done to determine the symmetry energy coefficients of dilute warm nuclear matter. The density range explored is up to $\sim 0.05\rho_0$, ρ_0 being the density of normal nuclear matter. The symmetry energy coefficients at these low densities are found to be significantly larger than those obtained from effective interactions [3–5] in the mean-field (MF) models. These results bear very interesting import in the astrophysical context. A higher symmetry energy, for example, would lead to a lower (e^-)-capture rate in the supernova collapse phase, which would result in a stronger explosive shock [6] and may thus significantly influence the initial conditions for the postbounce evolution of the supernova. The isotopic abundance of the relatively heavy elements produced in explosive nucleosynthesis is also directly influenced by the symmetry energy.

The experimental observations, more or less, matched the theoretically predicted trend made earlier by Horowitz and Schwenk [7] for the symmetry energy coefficients of dilute nuclear matter. They had made a virial treatment of the said matter and found from the free-energy considerations that the matter, if assumed to be a system of interacting gas of nucleons and nucleon-clusters, is more stable compared to pure nucleonic matter. For simplicity, they considered the matter to be composed of nucleons and alphas only. Soon afterward, the S-matrix approach [8] as applied to dilute nuclear matter was developed [9]. This approach provides a fully consistent logical framework for describing the thermodynamic properties of dilute hadronic matter. In its rudimentary form this goes over to the virial equation of state of Horowitz and Schwenk, which is an extension of the Beth-Uhlenbeck [10] scheme to include bound and scattering states of systems heavier than the two-nucleon system in the virial treatment. Calculations [4,11] in this approach again produced values of the symmetry energy coefficients much larger than those obtained in the MF models and are seen to be in reasonable consonance with the experimental trend.

The aim of the present article is to have a closer look at the evaluation of symmetry energy or symmetry free-energy coefficients of dilute nuclear matter. There are different definitions of symmetry energy coefficients available in the literature. For pure nucleonic matter below ρ_0 at any temperature T, the near-perfect linearity of the per particle energy $E(\rho, X, T)$ in X^2 [4,12] [$X = (\rho_n - \rho_p)/(\rho_n + \rho_p)$ is the nuclear asymmetry parameter] makes these definitions practically equivalent. Energy of clusterized nuclear matter, however, shows a different behavior with X. A resulting ambiguity in the definition of the symmetry energy coefficients is addressed in this article. We also find that the experimentalists resort to different approximations in evaluating the density and temperature of the clusterized matter produced and take the help of isoscaling to determine [1,2] the symmetry energy coefficients of the said matter at the specified density and temperature. From the S-matrix-based cluster composition of dilute nuclear matter at finite temperature followed by sequential decay [13], we try to understand the veracity of these approximations and apply the different definitions including isoscaling techniques [14–16] to evaluate the symmetry energy coefficients and compare with the experimental data.

The article is organized as follows. The various theoretical details are presented in Sec. II. The results and discussions are contained in Sec. III. The concluding remarks are given in Sec. IV.

II. THEORETICAL ELEMENTS

The definition of symmetry energy coefficients of dilute nuclear matter is not unique. In Sec. II A, definitions commonly used in the literature are given. In Sec. II B, a brief outline of the S-matrix framework is presented within which the symmetry coefficients with these definitions are evaluated. In Sec. II C, expressions for a few relevant observables are given. Determination of the symmetry coefficients of clusterized matter requires the knowledge of the source temperature and also of the primary fragment multiplicities. The experimentally detected multiplicities are the ones that have undergone secondary particle emission. In Sec. II D, we show how to correlate the detected multiplicities to the primary ones and how the temperature of the fragmenting system is obtained from the double ratio of the modified isotope yield. This makes

*jn.de@saha.ac.in
†santosh.samaddar@saha.ac.in
‡bijay.agrawal@saha.ac.in

the extraction of the symmetry coefficients from isoscaling techniques more reliable.

A. The symmetry energy coefficient

The symmetry energy of an asymmetric nuclear system is defined as the energy change in making the system isospin symmetric. For a homogeneous system, microscopic calculations in the mean-field model [17] show that the energy per nucleon of asymmetric nuclear matter up to saturation density is practically linear in X^2 and may be written as $E(\rho, X, T) = E(\rho, X = 0, T) + C_E(\rho, T)X^2$. The term $C_E(\rho, T)X^2$ is the symmetry energy $E_{\rm sym}$, and the slope parameter C_E is called the symmetry coefficient. In the nuclear mass formula for the binding energy per particle, the symmetry energy also appears as a term $C_E X^2$. Empirical values of C_E are found to be ∼23–25 MeV for medium-heavy nuclei compared to ∼30–34 MeV for nuclear matter at the saturation density because of surface effect. The symmetry coefficient C_E was defined in several ways:

$$C_E(\rho, T) = [E(\rho, X, T) - E(\rho, X = 0, T)]/X^2, \quad (1)$$

$$C_E(\rho, T) = [E(\rho, X = 1, T) + E(\rho, X = -1, T)]/2 - E(\rho, X = 0, T), \quad (2)$$

and

$$C_E(\rho, T) = \frac{1}{2}\left(\frac{\partial^2 E(\rho, X, T)}{\partial X^2}\right)_{X=0}. \quad (3)$$

For uniform nuclear matter at densities up to saturation, all three definitions yield nearly the same value of C_E as $E(X)$ is seen to be nearly linear in X^2 in the whole range of X. Similar definitions follow for the symmetry free-energy coefficient C_F, namely, $F(\rho, X, T) = F(\rho, X = 0, T) + C_F X^2$ where $F(\rho, X, T)$ denotes the free energy. For dilute nuclear matter in equilibrium, however, the system finds minimum free energy when it is clusterized. The clusterized fragments, even for symmetric dilute nuclear matter may not be all symmetric; they may thus contribute sizable symmetry energy to the total energy of the system. The total energy or free energy of the asymmetric system may then deviate considerably from the linearity in X^2; this makes an unambiguous definition of the symmetry coefficients C_E or C_F difficult.

Experimentally, the nuclear symmetry energy coefficients have been extracted from isoscaling [1,2]. From measured fragment yields $Y_i(N, Z)$ from two similar fragmenting systems $i = 1, 2$ differing in isospin content, a scaling relation,

$$Y_2(N, Z)/Y_1(N, Z) \propto e^{\delta N + \gamma Z}, \quad (4)$$

was observed. In the model of nuclear statistical equilibrium (NSE) [18], the isoscaling parameters are given by $\delta = (\mu_{n_2} - \mu_{n_1})/T$ and $\gamma = (\mu_{p_2} - \mu_{p_1})/T$ where μ_{n_i}'s and μ_{p_i}'s are the neutron and proton chemical potentials in the two systems. From the measured multiplicities of different isotopes of any specific element, say, δ can be extracted experimentally and then the symmetry free-energy coefficient C_F is related to δ as [15]

$$C_F = \frac{\delta T}{4\left[(Z/A)_1^2 - (Z/A)_2^2\right]}, \quad (5)$$

where $(Z/A)_i$ are the proton fractions in the two systems. The symmetry energy coefficient C_E is then evaluated as

$$C_E = C_F + TC_S, \quad (6)$$

where C_S is the symmetry entropy coefficient; it is defined as $C_S = [S(\rho, X, T) - S(\rho, X = 0, T)]/X^2$, where S is the entropy per nucleon evaluated using the theoretical model [1,2].

In an explosive supernova scenario, Def. I may possibly find its use. There, the physical process involves, in general, changes in density, temperature, and isospin asymmetry. One has to deal with quantities like $\Delta F = F(\rho_2, X_2, T_2) - F(\rho_1, X_1, T_1)$. After rearrangement, ΔF can be written as

$$\begin{aligned}\Delta F = {} & [F(\rho_2, X_2, T_2) - F(\rho_2, X = 0, T_2)] \\ & - [F(\rho_1, X_1, T_1) - F(\rho_1, X = 0, T_1)] \\ & + [F(\rho_2, X = 0, T_2) - F(\rho_1, X = 0, T_2)] \\ & + [F(\rho_1, X = 0, T_2) - F(\rho_1, X = 0, T_1)]. \end{aligned} \quad (7)$$

The previous equation reduces to

$$\Delta F = \left[C_F(\rho_2, X_2, T_2)X_2^2 - C_F(\rho_1, X_1, T_1)X_1^2\right] + \int_{\rho_1}^{\rho_2} \frac{P(\rho, X = 0, T_2)}{\rho^2} d\rho - \int_{T_1}^{T_2} S(\rho_1, 0, T) dT. \quad (8)$$

In Eq. (8), $C_F(\rho, X, T)$ is the asymmetry-dependent free symmetry energy coefficient as defined through Def. I, $P(\rho, X = 0, T)$ is the pressure of symmetric dilute nuclear matter, and S is its entropy per nucleon.

B. The *S*-matrix framework

The S-matrix formalism in the nuclear context was already presented in some detail in Refs. [9] and [11]. For the sake of completeness, we give below some of its salient features.

The grand partition function of an interacting infinite system of neutrons and protons can be written as

$$\mathcal{Z} = \sum_{Z,N=0}^{\infty} (\zeta_p)^Z (\zeta_n)^N \, {\rm Tr}_{Z,N} \, e^{-\beta H}. \quad (9)$$

Here, ζ's are the elementary fugacities, $\zeta_n = e^{\beta\mu_n}$ and $\zeta_p = e^{\beta\mu_p}$ with $\beta = 1/T$ the inverse of the temperature, and μ's are the nucleonic chemical potentials. H is the total Hamiltonian of the system and ${\rm Tr}_{Z,N}$ is taken over states of Z protons and N neutrons. The dynamical information concerning the nucleonic interaction is contained in the partition function as two types of terms [8],

$$\ln \mathcal{Z} = \ln \mathcal{Z}_{\rm part}^{(0)} + \ln \mathcal{Z}_{\rm scat}. \quad (10)$$

The first term on the right-hand side corresponds to contributions from stable single-particle states of clusters of different sizes including neutrons and protons formed in the system; the second term refers to all possible scattering states. The

superscript (0) indicates that the clusters behave as an ideal quantum gas. The first term includes contributions from both the ground states of the clusters and their excited states below the particle emission threshold so that

$$\ln \mathcal{Z}^{(0)}_{\rm part} = \ln \mathcal{Z}^{(0)}_{\rm gr} + \ln \mathcal{Z}^{(0)}_{\rm ex}\,, \tag{11}$$

with

$$\ln \mathcal{Z}^{(0)}_{\rm gr} = \mp V \sum_i g^i_0 \int \frac{d\mathbf{p}}{(2\pi)^3} \times \ln\left(1 \mp \zeta_i e^{-\beta(p^2/2A_i m)}\right), \tag{12}$$

and

$$\ln \mathcal{Z}^{(0)}_{\rm ex} = \mp V \sum_i \sum_{\epsilon^i_j=\epsilon^i_1}^{\epsilon^i_s} g^i_j \times \int \frac{d\mathbf{p}}{(2\pi)^3} \ln\left(1 \mp \zeta_i e^{-\beta(p^2/2A_i m+\epsilon^i_j)}\right). \tag{13}$$

In Eqs. (10) and (11), i refers to a fragment species with mass, charge, and neutron number A_i, Z_i, and N_i, respectively. The upper and lower signs refer to bosonic and fermionic clusters with $g^i_0(g^i_j)$ as the ground-state (excited-state) spin degeneracies and V is the volume of the system. The effective fugacity ζ_i is $\zeta_i = e^{\beta(\mu_i+B_i)}$ where from chemical equilibrium $\mu_i = N_i\mu_n + Z_i\mu_p$ and B_i is the binding energy of the cluster. Here $\mathbf{p}$ is the momentum of the cluster and m is the nucleonic mass. A nucleus in a particular excited state is taken as a distinctly different species and can be treated in the same footing as the ground state. In Eq. (11), the sum is taken over all particle-stable excited states and for $A \leqslant 16$, all the discrete particle-stable excited states [13,19,20] are included. For $A > 16$, the sum in Eq. (11) is replaced by an integral weighted with the level density $\omega(A,\epsilon^*)$, the integral extending from the first excited state ϵ^i_1 taken to be 2 MeV to the particle emission threshold energy ϵ^i_s, taken as 8 MeV, both ϵ^i_1 and ϵ^i_s being taken to be independent of the species. Equation can then be recast as

$$\ln \mathcal{Z}^{(0)}_{\rm ex} = \mp V \sum_i \int_{\epsilon^i_1}^{\epsilon^i_s} d\epsilon^* \omega(A,\epsilon^*) \times \int \frac{d\mathbf{p}}{(2\pi)^3} \ln\left(1 \mp \zeta_i e^{-\beta(p^2/2A_i m+\epsilon^*)}\right). \tag{14}$$

The expression for the level density is taken from Ref. [21].

The scattering term in Eq. (10) may be written as a sum of contributions from a set of channels with total proton number Z_t, neutron number N_t, and mass number A_t. All the other labels required to fix a channel is denoted by σ. The scattering term can then be written as

$$\ln \mathcal{Z}_{\rm scat} = V \sum_{Z_t,N_t} \frac{A_t^{3/2} e^{\beta\mu_{Z_t,N_t}}}{\lambda_N^3} \sum_\sigma e^{\beta B_{Z_t,N_t,\sigma}} \times \int_0^\infty d\epsilon \frac{e^{-\beta\epsilon}}{2\pi i} \mathrm{Tr}_{Z_t,N_t,\sigma}\left(\mathcal{A}S^{-1}(\epsilon)\frac{\partial}{\partial\epsilon}S(\epsilon)\right)_c, \tag{15}$$

the trace being restricted to channel (Z_t, N_t, σ). In Eq. (15) $\lambda_N = h/\sqrt{2\pi m T}$ is the nucleon thermal wavelength and ϵ is the center-of-mass kinetic energy in the channel. Here $\mathcal{A}$ represents the bosonic symmetrization or fermionic antisymmetrization operator, S is the scattering operator, and the subscript c, in diagrammatic language, refers only to the connected part of the expression in the parenthesis. The quantity $B_{Z_t,N_t,\sigma}$ is the sum of the individual binding energies of all the particles participating in the scattering channel. From binding energy considerations, two-particle channels are expected to be more dominant than the multiparticle channels for any particular Z_t and N_t. We thus consider only two-particle scattering channels. In essence, the interactions among the nucleons are contained in the ground and excited states of the clusters and all the possible scatterings between them. The scattering contribution to the partition function is split into two parts, one coming from the low mass particles ($A \leqslant 8$, say) and the other from heavy ones, containing at least one high mass particle ($A > 8$), so that we write,

$$\ln \mathcal{Z}_{\rm scat} = \ln \mathcal{Z}^L_{\rm scat} + \ln \mathcal{Z}^H_{\rm scat}. \tag{16}$$

Because the scattering of relatively heavier nuclei is known to be dominated by a multitude of narrow resonances near the continuum threshold, the S-matrix elements for them are approximated by resonances, each of which can be treated [22,23] like an ideal gas term. For heavier mass fragments $A > 16$, assuming the resonance level densities to be the same as that of excited states below threshold, the scattering contribution from the heavier mass fragments $\ln \mathcal{Z}^H_{\rm scat}$ takes the form similar to that in Eq. (14) where the integration interval ϵ^i_1 to ϵ^i_s over the excitation energy is replaced by ϵ^i_s to ϵ^i_r, ϵ^i_r being the limit of resonance domination. For $A \leqslant 16$, in Eq. (11) the sum over all the particle-decaying excited states are taken with lifetimes >200 fm/c.

For $\ln \mathcal{Z}^L_{\rm scat}$, only the scattering channels NN, Nt, N^3He, $N\alpha$ and $\alpha\alpha$ are considered, where N and t refer to the nucleon and the triton, respectively. Then

$$\ln \mathcal{Z}^L_{\rm scat} = \ln \mathcal{Z}_{NN} + \ln \mathcal{Z}_{Nt} + \ln \mathcal{Z}_{N^3\mathrm{He}} + \ln \mathcal{Z}_{N\alpha} + \ln \mathcal{Z}_{\alpha\alpha}. \tag{17}$$

Each of the terms in Eq. (17) can be expanded in the respective virial coefficients. Expansion up to the second-order coefficients are only considered; they are written as energy integrals of the relevant phase shifts [7,9]. Collecting the various contributions, the grand partition function takes the form,

$$\ln \mathcal{Z} = \ln \mathcal{Z}^{(0)}_{\rm gr} + \ln \mathcal{Z}^{(0)}_{\rm ex} + \ln \mathcal{Z}^L_{\rm scat} + \ln \mathcal{Z}^H_{\rm scat}. \tag{18}$$

C. Expressions for some relevant observables

The explicit expression for the partition function given by Eq. (18) is

$$\ln \mathcal{Z} = V \left\{ \frac{2}{\lambda_N^3}\left[\zeta_n + \zeta_p + \frac{b_{nn}}{2}\zeta_n^2 + \frac{b_{pp}}{2}\zeta_p^2 + \frac{1}{2}b_{np}\zeta_n\zeta_p\right] + \frac{2}{\lambda_t^3}[\zeta_t + 2\zeta_t(b_{pt}\zeta_p + b_{nt}\zeta_n)]\right.$$

$$+\frac{2}{\lambda_h^3}[\zeta_h + 2\zeta_h(b_{ph}\zeta_p + b_{nh}\zeta_n)]$$
$$+\frac{1}{\lambda_\alpha^3}\left[\zeta_\alpha + b_{\alpha\alpha}\zeta_\alpha^2 + b_{n\alpha}\zeta_\alpha(\zeta_n+\zeta_p)\right]$$
$$+\sum_i \frac{\zeta_i}{\lambda_i^3}\left(g_0^i + \sum_{\epsilon_j^i=\epsilon_1^i}^{\epsilon_r^i} g_j^i e^{-\epsilon_j^i/T}\right)\Bigg\}. \quad (19)$$

The sum in the parenthesis of the last term in Eq. (19) goes over to an integral for $A > 16$ as stated earlier. The subscripts n, p, t, h, and α refer to the neutron, proton, triton, ^{3}He, and ^{4}He, respectively, and λ_i is the thermal wavelength ($\lambda_i = \lambda_N/\sqrt{A_i}$) of a fragment species i with mass mA_i. The b_{nn}, etc., are the temperature-dependent virial coefficients. The model with the partition function given by Eq. (19) will be referred to as the S-matrix (SM) model; the neglect of the scattering terms (the terms involving the virial coefficients) leads to the NSE model. Further neglect of the excited states as used by Albergo *et al.* [24] in the context of isotope thermometry will be referred to as the NSE0 model. Once the partition function is known, all the relevant observables can be calculated.

The pressure can be evaluated from

$$P = T\ln\mathcal{Z}/V. \quad (20)$$

The number density ρ_i of the ith fragment species is calculated from

$$\rho_i = \zeta_i\left(\frac{\partial}{\partial\zeta_i}\frac{\ln\mathcal{Z}}{V}\right)_{V,T}. \quad (21)$$

For relatively low density and not too low temperature, the fugacity $\zeta \ll 1$. The quantal distribution can then be well approximated by the classical one. The primary fragment multiplicity densities for the ith species can then be derived as

$$\rho_i = \frac{1}{\lambda_i^3}e^{[\mu_i N_i+\mu_p Z_i+B(A_i,Z_i)]/T} \times\left(g_0^i + \sum_{\epsilon_j=\epsilon_1^i}^{\epsilon_r^i} g_j^i e^{-\epsilon_j^i/T}\right) + \rho_{sc}^i. \quad (22)$$

In Eq. (22), the sum over the excited states includes both the γ and particle-decay (resonance) channels. The last term ρ_{sc}^i is the contribution to the fragment yield from scattering; it is nonzero only for the fragments with $A \leqslant 4$, the explicit expressions for which are given in Ref. [7]. The sum in the parenthesis in Eq. (22) goes over to an integral for $A > 16$ as mentioned before.

The free-energy density is then calculated from the Gibbs-Duhem relation,

$$\mathcal{F} = -P + \sum_i \mu_i\rho_i. \quad (23)$$

The entropy density is

$$\mathcal{S} = \left(\frac{\partial P}{\partial T}\right)_\mu, \quad (24)$$

which yields the total energy density as

$$\mathcal{E} = \mathcal{F} + T\mathcal{S}. \quad (25)$$

The full expression for the entropy density is

$$\mathcal{S} = \frac{5}{2}\frac{P}{T} - \sum_i \rho_i\ln\zeta_i + \frac{T}{\lambda_N^3}\left\{\zeta_n\zeta_p b_{np}^{0\prime} + (\zeta_n^2+\zeta_p^2)b_{nn}'\right\} + \frac{4T}{\lambda_t^3}\zeta_t\{\zeta_n b_{nt}' + \zeta_p b_{pt}'\} + \frac{4T}{\lambda_h^3}\zeta_h\{\zeta_n b_{nh}' + \zeta_p b_{ph}'\} + \frac{T}{\lambda_\alpha^3}\left\{\zeta_\alpha^2 b_{\alpha\alpha}' + \zeta_\alpha(\zeta_n+\zeta_p)b_{n\alpha}'\right\} + \frac{1}{T}\sum_{i\in H}\frac{\zeta_i}{\lambda_i^3}\int\omega(\epsilon^*)\epsilon^* e^{-\epsilon^*/T}d\epsilon^*, \quad (26)$$

where $\sum_i$ denotes the sum over all the species and $\sum_{i\in H}$ signifies that the sum runs over the channels of heavy fragments.The primes on the virial coefficients denote their temperature derivatives. The coefficient b_{np}^0 corresponds to the nonresonance n-p scattering contribution; it is related to the full b_{np} as $b_{np} = b_{np}^0 + b_d$ with $b_d = 6\sqrt{2}e^{B_d/T}$, B_d being the binding energy of deuteron.

D. Connecting measured data to primary observables

Experimental extraction of the symmetry free-energy coefficient from isoscaling depends on the knowledge of the temperature T of the disassembling source and the isoscaling parameters δ and/or γ. They, in turn, are determined exploiting the multiplicity distribution of the excited primary fragments. Because of subsequent particle emission, however, the primary distribution changes leading to secondary yield of the fragments. Experimentally, the latter are measured, reconstruction of the primary multiplicities from the experimentally detected ones is then necessary to get T, δ, and γ and also the other thermodynamic parameters at the time of nuclear disassembly (freeze-out). This was discussed in Ref. [13]; here we present it in brief for completeness.

The observed secondary yield of light fragments ($A_i \leqslant 4$, $Z_i \leqslant 2$), because of feeding from excited heavier ones, can be written in terms of thermodynamic parameters V, μ_n, μ_p, and T at freeze-out as

$$Y_i(A_i,Z_i) = Vg_0^i\frac{A_i^{3/2}}{\lambda_N^3}e^{[(N_i\mu_n+Z_i\mu_p+B(A_i,Z_i))/T]} + V\sum_j\sum_{k_j}\left\{\frac{A_j^{3/2}}{\lambda_N^3}e^{[(N_j\mu_n+Z_j\mu_p+B(A_j,Z_j))/T]} \times\omega_p^{k_j}(A_j,Z_j,T)x_i^{k_j}(A_j,Z_j,T)\right\} + V\rho_{sc}^i. \quad (27)$$

In Eq. (27), the first and last terms together comprise the primary multiplicities of the said light fragments; the middle term represents their population growth from decay of heavier species. The quantity $x_i^{k_j}$ corresponds to the branching ratio of the kth particle-decaying state of the jth heavy species

for emitting the light ith species. It is calculated using the Weisskopf-Ewing model [25]. The quantity $\omega_p^{k_j}(A_j, Z_j, T)$ is the internal partition function for the particle-unstable states,

$$\omega_p^{k_j}(A_j, Z_j, T) = g_k^j e^{-\epsilon_k^j/T}. \tag{28}$$

For heavy particles ($A > 4$, $Z \geqslant 2$), the experimentally observed yield is written as

$$\begin{aligned} Y(A, Z) = V \frac{A^{3/2}}{\lambda_N^3} e^{(N\mu_n + Z\mu_p + B(A,Z))/T} \\ \times \left\{ g_0(A) + \omega_\gamma(A, Z, T) + \sum_{k_j} \sum_{i=1}^{6} \right. \\ \times \left(\frac{A + a_i}{A} \right)^{3/2} e^{(n_i\mu_n + z_i\mu_p + B(A+a_i, Z+z_i) - B(A,Z))/T} \\ \left. \times \omega_p^{k_j}(A + a_i, Z + z_i, T) x_i^{k_j}(A + a_i, Z + z_i, T) \right\}. \end{aligned} \tag{29}$$

In Eq. (29), $\omega_\gamma = \sum_k g_k e^{-\epsilon_k/T}$ is the partition function for γ-decaying states of the heavier fragments; the sum i runs over the emitted ejectiles, for which we take only $n, p, d, t, {}^3\mathrm{He}$, and α, a_i and z_i being their mass and charge. Given a set of experimental yields for four fragments, their single ratios are constructed using Eqs. (27) and (29), resulting in a system of three independent equations. Using the Newton-Raphson method, the equations can be solved iteratively for μ_n, μ_p, and T; the volume V can then be determined from the total observed yield of a fragment. Once these thermodynamic parameters are known, the primary yield can be easily calculated.

III. RESULTS AND DISCUSSIONS

As mentioned earlier, the definition of the symmetry energy coefficients C_E and C_F for clusterized nuclear matter is not unique; their values may depend on the prescriptions used to evaluate them. In this article, we calculate the symmetry coefficients for warm dilute nuclear matter at different temperatures and densities using several prescriptions as used in the literature for uniform matter; we employ the S-matrix framework for this purpose. To examine critically the role of clusterization on the symmetry coefficients, we also evaluate them in the relativistic mean-field model (RMF) for uniform nucleonic matter. Finally, the calculated coefficients are compared with the experimental values [2] of C_E and C_F, extracted recently exploiting the phenomenon of isoscaling [15]. Hereafter, the definitions of C_E given by Eqs. (1)–(3) will be referred to as Def. I, Def. II, and Def. III, the definition given by Eqs. (5) and (6) from isoscaling will be referred to as Def. IV. Analogous definitions follow for the symmetry free-energy coefficient C_F.

As already mentioned, the symmetry energies of dilute clusterized nuclear matter may deviate considerably from the linearity in X^2. In Fig. 1, the symmetry energy and free energy per nucleon of dilute neutron-rich matter evaluated in the SM model are presented as black lines at densities $\rho = 0.002$ and 0.02 fm^{-3} and at temperatures of $T = 4$ and 8 MeV as a function of X^2. The calculations in the left panels [(a) and (c)] refer to those at the lower temperature $T = 4$ MeV, those on the right panels [(b) and (d)] correspond to calculations at $T = 8$ MeV. In these calculations, the maximum mass of the fragment $A_{\max}$ allowed to be formed in the dilute matter is taken as 50; it is found that the results with $A_{\max} = 20$ is almost the same as those for $A_{\max} = 50$ as at these densities and temperatures formation of a fragment with mass > 20 is not very significant. The full and dashed lines refer to calculations at densities $\rho = 0.002$ and 0.02 fm^{-3}, respectively. The results are seen to be nonlinear in X^2, the nonlinearity depending on ρ and T. To visualize the effects of clusterization on the behavior of symmetry energies, we compare our results with those obtained for the uniform nucleonic matter. The results for uniform matter as depicted in Fig. 1 (red solid and dashed lines) have been calculated using the BSR4 parameter set [26,27] of the extended RMF model [28–30]. The BSR4 parameter set satisfies simultaneously the empirical constraint on the density dependence of the symmetry energy as well as the experimental data on the bulk properties of finite nuclei as was recently shown [27]. The symmetry energies and free energies calculated in the RMF model are seen to be always smaller than those obtained in the SM approach. The calculated symmetry energies here are practically linear in X^2, however, the symmetry free energies have a nonlinear component. For an estimate of this nonlinearity in the symmetry energies, a quartic term in the asymmetry parameter X is added to E_{sym} and F_{sym} as $E_{\mathrm{sym}} = a_e X^2 + b_e X^4$ and $F_{\mathrm{sym}} = a_f X^2 + b_f X^4$. The coefficients a and b are dependent on ρ and T and are obtained by a least-squares fit to the calculated values at different values of X. For a quantitative feeling of this nonlinearity, the values of the coefficients a and b at densities $\rho = 0.002$ and 0.02 fm^{-3} and at temperatures $T = 4$ and 8 MeV are presented in Table I for the results calculated in both the SM and RMF

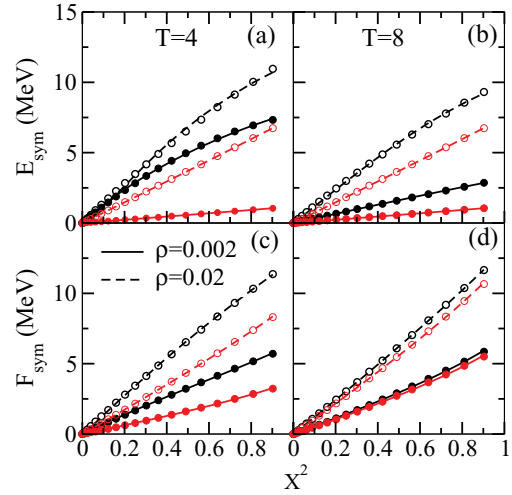

FIG. 1. (Color online) The symmetry energy E_{sym} and symmetry free energy F_{sym} displayed as a function of X^2. The black lines [top two lines (a); top and middle lines (b)–(d)] correspond to calculations in the SM model; the red lines [bottom two lines (a); middle and bottom lines (b)–(d)] are the ones obtained in RMF theory. The solid and open circles depict the least-squares fitted values with a quartic term in X in the expressions for E_{sym} and F_{sym}.

TABLE I. The least-squares fitted coefficients a and b at different temperatures T and densities ρ. The coefficients and T are in MeV and ρ is in fm^{-3}.

Model	T	ρ	a_e	b_e	a_f	b_f
SM	4	0.002	12.517	−4.879	6.860	−0.601
	4	0.02	14.607	−2.733	14.168	−1.743
	8	0.002	3.300	−0.146	5.212	1.424
	8	0.02	12.611	−2.541	11.864	1.163
RMF	4	0.002	1.129	0.038	2.920	0.727
	4	0.02	7.303	0.188	8.424	0.868
	8	0.002	1.129	0.038	4.829	1.416
	8	0.02	7.303	0.188	10.411	1.565

models. It is seen that the coefficients b_e in the RMF model are quite small compared to a_e indicating the near linearity of the symmetry energy in X^2 in this model; in the SM model these coefficients are appreciably larger. The fitted values are shown as solid and open circles for the lower and the higher densities, respectively. With the quartic term, the fit to the calculated results are seen to be as a whole excellent for the temperatures and densities studied.

In Fig. 2, the calculated values of symmetry coefficients C_E and C_F in Def. I at three temperatures $T = 4$, 6, and 8 MeV for densities up to $\rho = 0.03$ fm^{-3} are displayed. The value of the asymmetry parameter X occurring in Eq. (1) is taken to be $X = 0.2$. The left panels [(a) and (b)] correspond to the values evaluated in the SM approach. Two characteristics for the symmetry coefficients are in general seen: (i) With increasing temperature, both C_E and C_F tend to decrease; (ii) with increasing density, they tend to level off. For the lowest temperature considered, however, C_E exhibits a peaked structure. The right panels [(c) and (d)] of Fig. 2 compare the values calculated in the SM (thick lines) and NSE models (thin lines) at $T = 4$ and 8 MeV. The effect of scattering is seen to

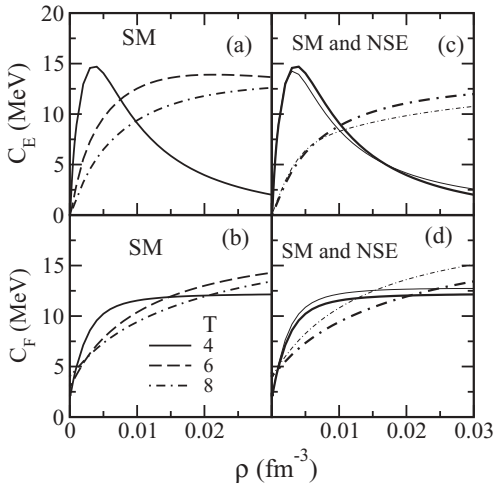

FIG. 2. The symmetry energy coefficients C_E and C_F calculated using Def. I as a function of density for the temperatures $T = 4$, 6, and 8 MeV. The left panels [(a) and (b)] correspond to calculations in the SM model. In the right panels [(c) and (d)], SM results (thick lines) are compared with those obtained in the NSE model (thin lines).

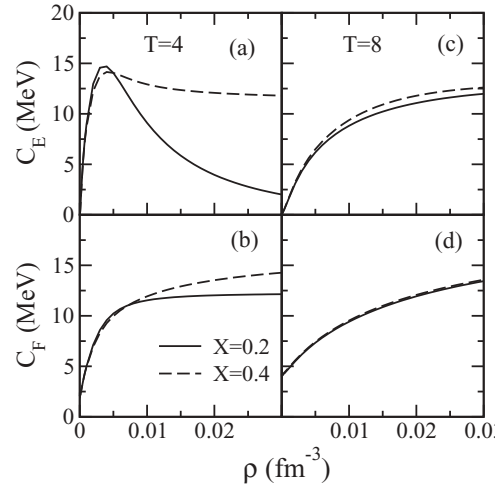

FIG. 3. The symmetry coefficients C_E and C_F obtained for different values of X using Def. I in the SM model shown as a function of density for $T = 4$ and 8 MeV.

be somewhat more visible at higher temperature; the larger density of lighter particles (n, p, etc.) in warmer systems is reflected here.

The values of C_E and C_F evaluated using Eq. (1) (Def. I) with two choices of the asymmetry parameter at $X = 0.2$ and $X = 0.4$ are displayed in Fig. 3 at two temperatures $T = 4$ and 8 MeV. While at higher temperature, the calculated values are not much different at different values of X [(c) and (d)], at the low temperature of 4 MeV quite different values for C_E and C_F are obtained as is seen from the solid and dashed lines in the left panels [(a) and (b)] of this figure with the notable feature that the peaked structure for C_E tends to wash out at higher values of X. The values of symmetry coefficients obtained from Def. I display a delicate interplay in the fragmentation pattern of dilute matter as a function density, temperature, and asymmetry; the peaked structure in C_E at $T = 4$ MeV and $X = 0.2$ is an outcome of this.

In Fig. 4, the values of C_E and C_F calculated in Def. II are presented at the same temperatures and in the same density

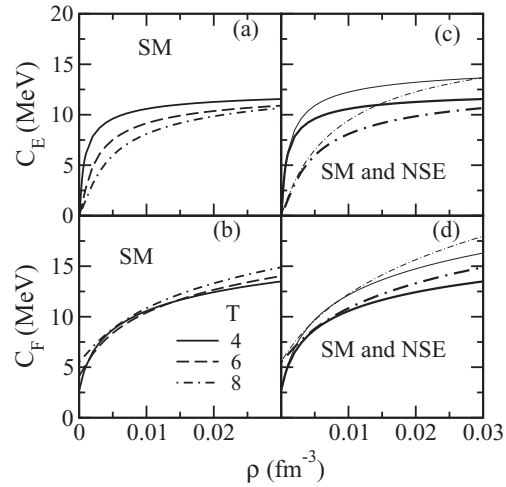

FIG. 4. Same as in Fig. 2 using Def. II.

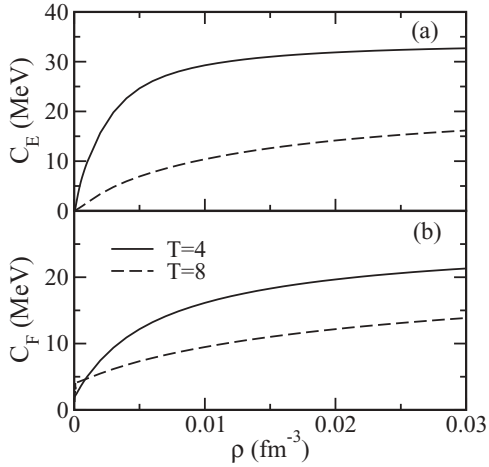

FIG. 5. The symmetry coefficients C_E and C_F obtained using Def. III at different densities at temperatures $T = 4$ and 8 MeV.

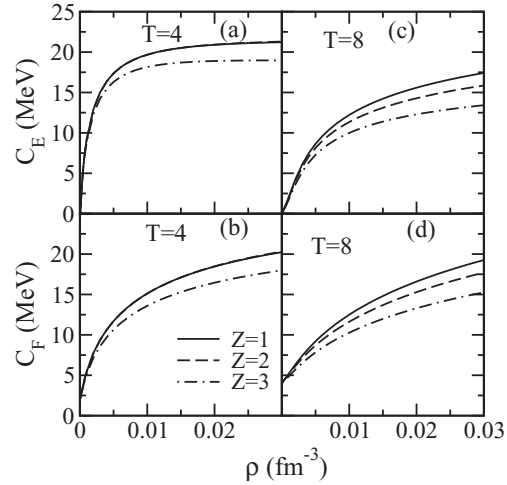

FIG. 6. The symmetry coefficients calculated as a function of density at $T = 4$ and 8 MeV in the SM model with inclusion of secondary decay employing isoscaling for isotopes of $Z = 1$, 2, and 3. The results for $Z = 1$ and 2 at $T = 4$ MeV are indistinguishable.

range as shown in Fig. 2 for Def. I. The symmetry coefficients increase with density and tend to saturate here, too. The symmetry free-energy coefficient C_F is seen to be nearly insensitive to temperature; C_E, however, is lower at higher temperatures, which is quite appreciable at low densities. This is a reflection of negative symmetry entropy in the density range we consider. Panels (c) and (d) of Fig. 4 display the effect of scattering on the symmetry coefficients; contrary to Def. I, this effect is more dominant here as one of the systems in the calculation of C_E or C_F is either pure neutron or proton matter.

In Fig. 5, the symmetry coefficients calculated using Eq. (3) (Def. III) are presented at $T = 4$ and 8 MeV as a function of density. Similar trends as with Def. I and Def. II are seen, however, the symmetry coefficients are found to be much larger. Similar display is done in Fig. 6 for the symmetry coefficients obtained in the isoscaling procedure (Def. IV). The twin fragmenting systems taken are at $X = 0.0$ and at $X = 0.2$. The fragments considered for the calculation are the isotopes of $Z = 1, 2$, and 3 obtained from the SM model. In the conventional isoscaling procedure, the symmetry coefficients are independent on the choice of atomic number Z; in our calculation, however, because of the presence of scattering and secondary decay from the excited primary fragments, a dependence on Z is observed. This is seen to be more prominent with increasing temperature and density. At the lower temperature of 4 MeV [(a) and (b)], the symmetry coefficients for $Z = 1$ and 2 are indistinguishable.

The extraction of C_F from isoscaling [Eq. (5)] is not unambiguous, it may have some dependence on the different sets of similarly prepared twin systems of proton fractions $(Z/A)_1$ and $(Z/A)_2$. This was addressed by calculating C_F with the choice of the two sets with twin systems ($X_1 = 0.0$, $X_2 = 0.1$) and ($X_1 = 0.0$, $X_2 = 0.2$). The results averaged over $Z = 1, 2, 3$ are presented in Fig. 7. The solid and dashed lines in red displayed in (b) and (d) [bottom two light lines] at temperatures $T = 4$ and 8 MeV refer to calculations in the NSE model without any secondary decay for the above two sets. A weak dependence on the choice of set is observed. The solid and dashed black lines refer to corresponding calculations in the SM model. The effects of scattering and decay are also seen not to be too strong. The calculated values of C_E at the two temperatures are displayed in (a) and (c). The dependence on the choice of set as well as on the scattering + secondary decay is seen to be very appreciable here.

A comparison of the symmetry coefficients evaluated employing the different definitions is made in Fig. 8. In Def. I and Def. IV, the asymmetric system is chosen with $X = 0.2$. Further calculations presented are done with this asymmetry. The symmetry coefficients calculated in the RMF model are shown as red lines. These results are always

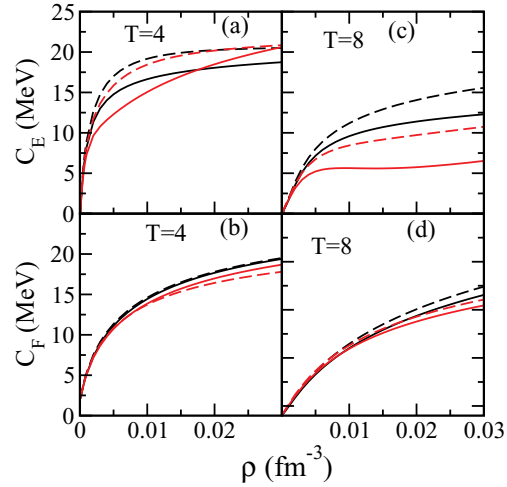

FIG. 7. (Color online) Effects of asymmetry and scattering + secondary decay on the symmetry coefficients employing isoscaling at $T = 4$ and 8 MeV. The solid and dashed lines correspond to twin fragmenting systems with ($X_1 = 0.0$, $X_2 = 0.1$) and ($X_1 = 0.0$, $X_2 = 0.2$) showing the asymmetry effect. The black lines represent calculations in the SM model with secondary decay; the red lines [middle and bottom light lines (a); bottom two light lines (b)-(d)] are the ones obtained without scattering and secondary decay.

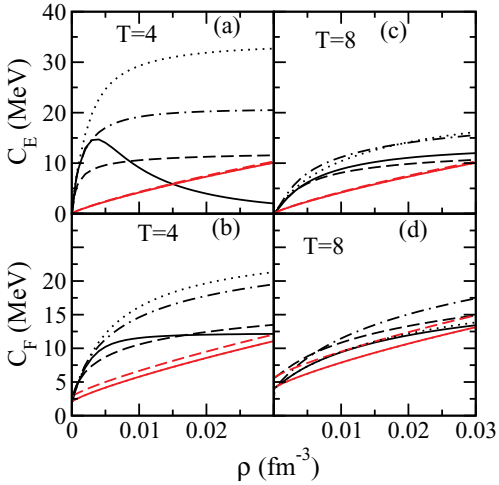

FIG. 8. (Color online) Comparison of the symmetry coefficients obtained with different definitions at different densities and temperatures. The solid, dashed, dotted, and dot-dashed lines correspond to calculations with Def. I, Def. II, Def. III, and Def. IV, respectively. The black lines are the results in the SM model; the red lines [the lines in light shade] are those obtained in the RMF model where results with Def. I and Def. III are indistinguishable.

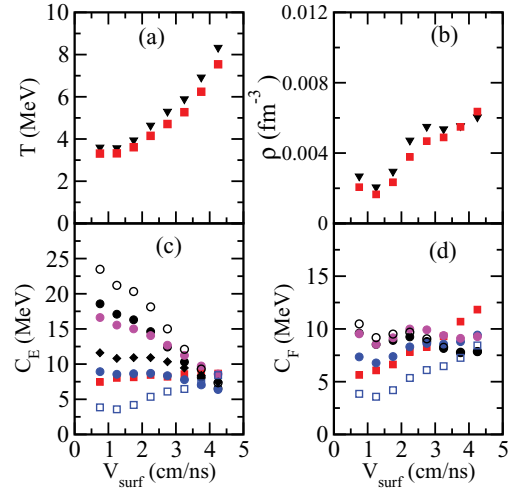

FIG. 9. (Color online) The extracted experimental values (red solid squares) of temperature and density from Ref. [2] are compared in (a) and (b) with the scattering-corrected values in the present calculations (inverted solid black triangles). In (c) and (d), the calculated symmetry coefficients in the SM model with Def. I, Def. II, and Def. IV (solid black, blue, and magenta circles [dark, light and lighter shades]), and Def. III (open circles) are compared with the experimental values (solid red squares). The solid diamonds in (c) correspond to C_E with C_F calculated in isoscaling, $S_{\rm sym}$ being evaluated with equivalent expression as used in Def. II. The open blue squares correspond to calculations in RMF using Def. II.

significantly lower than those obtained for clusterized matter showing the important role played by clusterization on the symmetry coefficients. At extremely low densities where the matter tends to be in a uniform nucleonic state, the different definitions yield more or less the same values for the symmetry coefficients for clusterized matter. In the RMF model, the coefficient C_E is practically independent on the choice of definition as symmetry energy is seen to be almost bilinear in X (see Fig. 1), however, the coefficient C_F is seen to be somewhat dependent on X as can be seen from the red solid lines (Def. I) and the dashed lines (Def. II) [the lines in light shade]. The coefficients obtained with Def. III in RMF are indistinguishable from those obtained with Def. I. The differences in the symmetry coefficients obtained with the different definitions for clusterized matter are found to be quite appreciable; the gaps are reduced with increasing temperature. At the lower temperature $T = 4$ MeV, the symmetry coefficients obtained with Def. III are seen to be the largest; those obtained from isoscaling (Def. IV) lie midway between those calculated using Def. III and the other two definitions. At higher temperature the dispersion among the various results obtained in different definitions narrows down.

Recent collision experiments with heavy ions have yielded values of the temperature and density of the hot dilute fragmenting nuclear matter and also its symmetry coefficients. In these experiments [2], multiplicities of the lighter particles, namely, n, p, d, t, ^{3}He, and ^{4}He have been measured. The temperature of the system was measured from isotope thermometry using the H-He thermometer based on the double-yield ratio $(t/d)/(^4\mathrm{He}/^3\mathrm{He})$ in the Albergo model [24]. In the same model, from single isotope ratio, the densities of the fragmenting source have been evaluated. In Figs. 9(a) and 9(b), they are shown as red solid squares [light shade] as a function of $v_{\rm surf}$ where $v_{\rm surf}$ is the velocity before the final Coulomb acceleration [2]. The Albergo model has no provision to consider the scattering effect on the thermodynamic observables; in the SM model, they are taken into account as detailed in Ref. [13]. Using the same H-He thermometer, from the input temperature and density obtained in the Albergo model, the scattering-corrected temperature and density are obtained iteratively. In (a) and (b), the corrected values of T and ρ are shown as inverted solid black triangles. Scattering correction is seen to have at most an $\sim$10% effect on these thermodynamic observables.

The calculated symmetry coefficients using different definitions are compared with the experimental ones in Figs. 9(c) and 9(d). The experimental values of the coefficient C_F were obtained using Eq. (5) with T and ρ as shown by the solid red squares [(a) and (b)]; the symmetry entropy was calculated in the NSE model with the equivalent expression of Eq. (2) as the difference between the entropies of pure neutron and proton matter and symmetric clusterized nuclear matter. The coefficient C_E was then obtained from Eq. (6). The solid black, blue, and magenta circles [dark, light and lighter shades] correspond to the present calculations in Def. I, Def. II, and Def. IV for clusterized matter in the SM approach with the scattering-corrected temperature and density, respectively. The open black circles represent corresponding results using Def. III. The different values of C_F shown in (d) reflect the nonuniqueness in their definition for clusterized dilute matter. They, however, remain in a moderately narrow band around the experimentally extracted values. The difference is amplified for the symmetry energy coefficient C_E as seen in (c). The solid black diamonds in (c) also represent the symmetry energy

coefficients calculated with Def. IV; their difference from the solid magenta circles is from the fact that in the former case, the symmetry entropy is calculated as the difference between pure neutron matter (instead of matter at $X = 0.2$) and symmetric matter as was done to extract the experimental values of C_E. The former choice of entropy calculation brings down the results considerably toward the experimental values. The open blue squares are the results obtained in the RMF model at the scattering-corrected temperatures and densities using Def. II. The results are not that sensitive to the choice of definition in this model as can be seen from Fig. 8. They are generally smaller compared to all other results including the experimental ones.

IV. CONCLUDING REMARKS

Finding out the symmetry coefficients of dilute nuclear matter as a function of temperature and density in the framework of the S-matrix approach was the primary aim in this article. Generally, it is found that the symmetry coefficients C_E and C_F increase with density at a fixed temperature and then they gradually tend to level off at a density of $\sim 0.2\ \rho_0$; the applicability of the SM approach may be doubtful beyond this density. At a fixed density, it is also seen that the symmetry coefficients decrease with temperature. The changing fragmentation pattern with density, temperature, and asymmetry makes the temperature dependence of the symmetry coefficients of dilute nuclear matter rather involved. A closed expression for the said temperature dependence is hard to find, unlike that for a finite nucleus [31]. At very low density, scattering effects on the symmetry coefficients are rather negligible; the effects become important with higher density and temperature. In the density domain we work in, the calculated symmetry coefficients in the SM approach are found to be generally considerably higher than those calculated for uniform nuclear matter.

We have taken recourse to the different definitions available in the literature for the evaluation of the symmetry coefficients of dilute warm nuclear matter that becomes nonhomogeneous and clusterized for stability. For uniform nuclear matter, these few definitions lead practically to the same values of the symmetry coefficients, but for the nonhomogeneous matter, different values are reached making a unique definition of the symmetry energy of dilute nuclear matter in terms of symmetry coefficients and asymmetry of the system difficult. Dilute symmetric nuclear matter is a case in point; the disassembled fragments may contribute to a sizable symmetry energy though the total asymmetry of the system is zero.

In trying to understand and compare our calculated values of the symmetry coefficients with the experimentally reported ones, we have made a modest attempt to critically analyze the extracted experimental parameters like density and temperature in our SM approach; we find that because of scattering effects (neglected in the experimental analyses), the temperature and densities are somewhat higher than those reported in experiments. The evaluated values of the symmetry free-energy coefficients at these experimental parameters are in reasonable consonance with those obtained from experiments. Compared to the symmetry free-energy coefficients, the symmetry energy coefficients are found to have a wider variation obtained in different definitions. The fragmentation pattern of a system is quite sensitive to its asymmetry parameter introducing a strong asymmetry dependence in the symmetry entropy coefficient C_S of Eq. (6). Different definitions of symmetry coefficients imply systems with different values of effective asymmetry producing a larger dispersion in C_E compared to C_F.

Examining the behavior of symmetry energies as a function of the asymmetry parameter X, it is evident that the symmetry coefficients of nonhomogeneous matter defined in the conventional way as $C_E \sim E_{\rm sym}/X^2$ or $C_F \sim F_{\rm sym}/X^2$ would be an involved function of X. Def. II and Def. III, by construction, are asymmetry independent; these definitions do not reflect the underlying functional behavior of the symmetry energy of nonhomogeneous matter on the asymmetry parameter. The symmetry coefficients obtained from isoscaling (Def. IV) have an implicit asymmetry dependence that may not be too large. They also have, as we have shown, dependence on the atomic numbers of the light fragment isotopes chosen for isoscaling because of the scattering and secondary decay effects. The experimental extraction of the symmetry coefficients, exploiting Def. IV, may thus depend on the experimental parameters. The symmetry coefficients obtained through Def. I are asymmetry dependent. In a real physical process such as the supernova collapse or explosive phase, as mentioned earlier, they are the ones that seem most useful in describing the changing physical entities in an evolving scenario of density, temperature, and asymmetry.

ACKNOWLEDGMENTS

J.N.D. and S.K.S. acknowledge support from the Department of Science and Technology, government of India.

[1] S. Kowalski *et al.*, Phys. Rev. C **75**, 014601 (2007).
[2] J. B. Natowitz *et al.*, Phys. Rev. Lett. **104**, 202501 (2010).
[3] B. A. Li, L. W. Chen, and C. M. Ko, Phys. Rep. **464**, 113 (2008), and references therein.
[4] J. N. De and S. K. Samaddar, Phys. Rev. C **78**, 065204 (2008).
[5] C. Fuchs and H. H. Wolter, Eur. Phys. J. A **30**, 5 (2006).
[6] A. W. Steiner, M. Prakash, J. M. Lattimer, and P. J. Ellis, Phys. Rep. **411**, 325 (2005).
[7] C. J. Horowitz and A. Schwenk, Nucl. Phys. A **776**, 55 (2006).
[8] R. Dashen, S.-K. Ma, and H. J. Bernstein, Phys. Rev. **187**, 345 (1969).
[9] S. Mallik, J. N. De, S. K. Samaddar, and S. Sarkar, Phys. Rev. C **77**, 032201(R) (2008).
[10] E. Beth and G. E. Uhlenbeck, Physica **4**, 915 (1937).
[11] S. K. Samaddar, J. N. De, X. Viñas, and M. Centelles, Phys. Rev. C **80**, 035803 (2009).
[12] J. Xu, L. W. Chen, B. A. Li, and H. R. Ma, Phys. Rev. C **75**, 014607 (2007).

[13] S. K. Samaddar and J. N. De, Phys. Rev. C **81**, 041601(R) (2010).
[14] H. S. Xu *et al.*, Phys. Rev. Lett. **85**, 716 (2000).
[15] A. Ono, P. Danielewicz, W. A. Friedman, W. G. Lynch, and M. B. Tsang, Phys. Rev. C **68**, 051601(R) (2003).
[16] C. B. Das, S. Das Gupta, W. G. Lynch, A. Z. Mekjian, and M. B. Tsang, Phys. Rep. **406**, 1 (2005).
[17] L. W. Chen, B. J. Cai, C. M. Ko, B. A. Li, C. Shen, and J. Xu, Phys. Rev. C **80**, 014322 (2009).
[18] B. S. Meyer, Annu. Rev. Astron. Astrophys. **32**, 153 (1994).
[19] F. Ajenberg-Selove, Nucl. Phys. A **490**, 1 (1988); **506**, 1 (1990); **523**, 1 (1991).
[20] D. R. Tilley, H. B. Weller, and C. M. Cheves, Nucl. Phys. A **564**, 1 (1993).
[21] A. Bohr and B. R. Mottelson, *Nuclear Structure*, Vol. I (W. A. Benjamin, Reading, 1969).
[22] R. Dashen and R. Rajaraman, Phys. Rev. D **10**, 694 (1974).
[23] R. Dashen and R. Rajaraman, Phys. Rev. D **10**, 708 (1974).
[24] S. Albergo, S. Costa, E. Costanzo, and A. Rubbino, Nuovo Cimento A **89**, 1 (1985).
[25] V. F. Weisskopf and P. H. Ewing, Phys. Rev. **57**, 472 (1940).
[26] S. K. Dhiman, R. Kumar, and B. K. Agrawal, Phys. Rev. C **76**, 045801 (2007).
[27] B. K. Agrawal, Phys. Rev. C **81**, 034323 (2010).
[28] R. Furnstahl, B. D. Serot, and H. B. Tang, Nucl. Phys. A **598**, 539 (1996).
[29] R. Furnstahl, B. D. Serot, and H. B. Tang, Nucl. Phys. A **615**, 441 (1997).
[30] B. D. Serot and J. D. Walecka, Int. J. Mod. Phys. E **6**, 515 (1997).
[31] S. J. Lee and A. Z. Mekjian, arXiv:1003.4864.